tvst

https://doi.org/10.1167/tvst.7.1.15

Article

Three-Dimensional Analysis of Peeled Internal Limiting Membrane Using Focused Ion Beam/Scanning Electron Microscopy

Akira Hirata[1,2], Kazuhisa Murata[3], Ken Hayashi[1], and Kei-ichiro Nakamura[2]

[1] Hayashi Eye Hospital, Fukuoka, Japan
[2] Division of Microscopic and Developmental Anatomy, Department of Anatomy, Kurume University School of Medicine, Kurume, Japan
[3] Department of Ophthalmology, Saga University Faculty of Medicine, Saga, Japan

Correspondence: Akira Hirata, Hayashi Eye Hospital, 4-23-35, Hakataekimae, Fukuoka 812-0011, Japan. e-mail: akhirata@gmail.com

Received: 12 July 2017
Accepted: 18 December 2017
Published: 2 February 2018

Keywords: internal limiting membrane; macular hole; epiretinal membrane; vitrectomy; focused ion beam/scanning electron microscopy

Citation: Hirata A, Kazuhisa M, Hayashi K, Nakamura K. Three-dimensional analysis of peeled internal limiting membrane using focused ion beam/scanning electron microscopy. Trans Vis Sci Tech. 2018; 7(1):15, https://doi.org/10.1167/tvst.7.1.15

Purpose: To reevaluate the effect of internal limiting membrane peeling during vitrectomy on the Müller cell damage, we examined the ultrastructure of the internal limiting membrane by using focused ion beam/scanning electron microscopy (FIB/SEM).

Methods: A total of 12 internal limiting membranes obtained during surgery in both the macular hole and the idiopathic epiretinal membrane groups were processed for observation by FIB/SEM. Three-dimensional structures of the internal limiting membrane were analyzed.

Results: The number of cell fragments in the macular hole group was 5.07 ± 1.03 per unit area of internal limiting membrane (100 μm^2). The total volume of cell fragments was 3.54 ± 1.24 μm^3/100 μm^2. In contrast, the number of cell fragments in the epiretinal membrane group was 12.85 ± 3.45/100 μm^2, and the total volume of cell fragments was 10.45 ± 2.77 μm^3/100 μm^2. Data for both values were significantly higher than those observed in the macular hole group ($P = 0.0024$ and $P = 0.0022$, respectively, Mann-Whitney U test). No statistical difference was found for the mean volume of the cell fragment between the two groups.

Conclusions: All of the internal limiting membrane examined in this study showed cell fragments on the retinal surface of the internal limiting membrane. As compared with macular hole, epiretinal membrane exhibited a higher number and total volume of cell fragments, indicating that internal limiting membrane peeling for epiretinal membrane might have a higher risk of causing inner retinal damage.

Translational Relevance: FIB/SEM was a useful tool for three-dimensional quantitative analysis of the internal limiting membrane.

Introduction

Peeling of the internal limiting membrane (ILM) is a procedure widely applied in surgeries for several macular disorders, such as macular hole (MH), epiretinal membrane (ERM), macular pucker, macular edema, and macular retinoschisis.[1–7] ILM peeling can increase the anatomical and functional success rates in surgery for MH, prevent the incidence of ERM recurrences, reduce macular thickness in refractory diffuse diabetic macular edema, and accelerate the improvement of myopic foveoschisis in high myopia.[7–10]

Anatomical and functional changes induced by ILM peeling have also been reported to be associated with the dissociated optic nerve fiber layer appearance observed during fundus examinations, concentric macular dark spots seen with optical coherence tomography (OCT), and the selective delay of the recovery of the focal macular b-wave in electroretinographic studies.[11–15] Direct evidence of Müller cell damage caused by ILM peeling is revealed by the appearance of cell fragments adhering to the retinal

side of the peeled ILM, which can be observed by transmission electron microscopy (TEM).[16–18]

Images obtained from the thin TEM sections, however, often fail to interpret the three-dimensional arrangement of the cell fragments. Although imaging using serial sections for TEM is one approach that has been used to overcome this problem, this method is still a lengthy and tedious process.

In 2008 focused ion beam/scanning electron microscopy (FIB/SEM) was introduced for use in analyzing biological specimens.[19] This device makes it possible to automatically and repeatedly use a constant thickness to mill the surfaces of the specimens, thereby allowing for the capture of the exposed surface by SEM.[20–22] As the images obtained are comparable to those observed by TEM, these can be used to create a cubic three-dimensional tissue structure with a maximal size of 100 μm.[19]

In this study, we attempted to quantitatively reveal the Müller cell damage caused by ILM peeling by using FIB/SEM to observe the three-dimensional ultrastructure of ILM obtained during surgery for idiopathic ERM and idiopathic MH. Furthermore, we also reevaluated the difference of the thicknesses for the peeled ILM, the number of the adhered cell fragments on the retinal surface of the ILM, and the volume of the cell fragments.

Materials and Methods

Patients

This study was carried out after providing an explanation of the benefit and the risk of the surgery, including the ILM peeling, to all of the participants. Informed consent was obtained from all of the patients after they read and signed the document that provided information on the collection of peeled ILM and its use for this research project. This research adhered to the tenets of the Declaration of Helsinki and was carried out in accordance with the guidelines of the Human Studies Committee of Hayashi Eye Hospital.

A total of 40 eyes of 40 patients recruited for the study underwent vitrectomy for the treatment of idiopathic MH or idiopathic ERM between January and July 2015. A total of 10 ILM specimens were collected from the MH group, and 30 specimens were collected from the ERM group. We then randomly selected six specimens from each of the two groups for analysis in the study. Clinical information for the patients was as shown in the Table. Briefly, the MH group consisted of three males and three females, with an average age of 65.8 ± 4.2 years. The MH was classified as stage 2 in three patients and stage 3 in the remaining three patients. Fundus and OCT examinations showed that none of these six patients exhibited any ERM formation on the retinal surface. The ERM group consisted of three males and three females, with an average age of 66.8 ± 6.5 years. Fundus examination showed that all patients exhibited apparent ERM, with the OCT revealing that the foveal thickness was more than 350 μm.

Surgeries were performed as follows. All patients underwent phacoemulsification and aspiration followed by the implantation of an intraocular lens. Subsequently, we then performed vitrectomy with a 25-gauge trocar system. After the core vitrectomy, artificial posterior vitreous detachment (PVD) was induced if PVD was not present. The peripheral vitrectomy was conducted under a wide-angle viewing system. After the application of brilliant blue G, ILM peeling was started from the area temporal to the macula, with the layer peeled away in a sheet that was two disc diameters in size.[23] In the ERM cases, both the ERM and the ILM were peeled together as one sheet (Figs. 1A, 1B). In the MH cases, after completion of ILM peeling, fluid–air exchange and air tamponade were then performed.

Specimen Preparation

Within 15 minutes after the ILM peeling, all specimens were immersion fixed in a mixture of 2.5% glutaraldehyde and 2% paraformaldehyde in 0.1 M cacodylate buffer (pH 7.4) for at least 2 hours and then stored for further preparation. The specimens were prepared as previously described.[24–26] Briefly, after washing five times with the cacodylate buffer, the specimens were postfixed for 30 minutes in a solution containing 2% osmium tetroxide and 1.5% potassium ferrocyanide in the cacodylate buffer at 4°C. The specimens were then washed five times with distilled water and immersed in 1% thiocarbohydrazide solution for 30 minutes. After washing with distilled water five times, the specimens were further immersed in 2% osmium tetroxide in distilled water and then washed five times with distilled water. Subsequently, after the specimens were en bloc stained in a solution of 4% uranyl acetate solution overnight for contrast enhancement, they were washed with distilled water. Specimens were further stained by Walton's lead aspartate solution for 1 hour.[27] After the staining, all specimens were dehydrated in an ethanol series, followed by infiltration of

Table. Patient Clinical Characteristics

Characteristics	MH ($n = 6$)	ERM ($n = 6$)
Gender, male/female	3:3	3:3
Age, y	65.6 ± 5.4	69.5 ± 7.8
Stage of MH, 2:3:4	3:3:0	N/A
Preoperative foveal thickness, μm	N/A	453.3 ± 41.6
Postoperative foveal thickness, μm	288.6 ± 22.1	338.3 ± 28.8[a]
Preoperative visual acuity, logMAR	0.49 ± 0.19	0.27 ± 0.10
Postoperative visual acuity, logMAR	0.12 ± 0.12[b]	0.06 ± 0.06[c]

[a] $P = 0.001$ compared with preoperative foveal thickness.
[b] $P = 0.004$ compared with preoperative visual acuity.
[c] $P = 0.003$ compared with preoperative visual acuity.

epoxy resin (Epon 812; TAAB Laboratories Equipment Ltd., Berkshire, UK) mixture, and polymerized for 72 hours at 60°C (Fig. 1C). The surface of the embedded specimens was exposed using a diamond knife on an Ultracut E microtome (Leica, Wetzlar, Germany). The resin blocks were then placed on the standard SEM microscope specimen holder for SEM imaging. The entire area of the specimens was divided into four quadrants, and we chose one area randomly in each quadrant for observation and quantitative analysis (Fig. 1C).

FIB/SEM Tomography and Three-Dimensional Structure Reconstruction

The exposed surface of the specimens was examined by backscatter electron imaging using a conventional field emission SEM with FIB (Quanta Three-Dimensional FEG; FEI, Eindhoven, The Netherlands). Serial images of the block face were acquired by repeated cycles of the milling and imaging of the surface using the Slice and View G2 operating software (FEI). Milling was performed with a gallium ion beam at 30 kV with a current of 15 nA. The milling pitch was set to 50 nm/step and 800 cycles. The images were acquired at a landing energy of 3 keV with a bias voltage of 1.5 kV. The resultant image stack was 25 × 35 × 40 μm of the block size and was processed using the ImageJ software (https://imagej.nih.gov/ij/; provided in the public domain by the National Institutes of Health, Bethesda, MD) and Amira software (v6.0.1; FEI Visualization Science Group, Burlington, MA). The ILM and the cell fragments were segmented semiautomatically in order to create the three-dimensional structures for observation. Subsequently, the outlined ILM and the cell fragments were visualized and displayed.

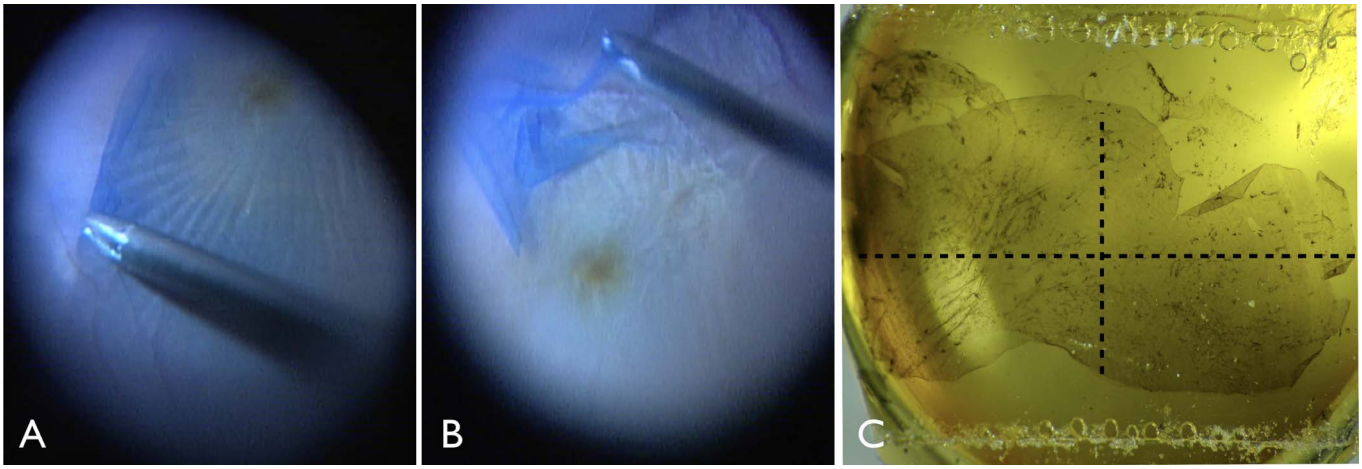

Figure 1. Intraoperative findings and the embedded specimen. (A, B) After the application of brilliant blue G, ILM peeling with the ERM was performed as one sheet. (C) ILM was embedded as a whole mount in epoxy resin. The entire area of the specimen was then divided into four quadrants (*dotted lines*), with one area in each quadrant chosen for analysis.

Measurement and Statistical Analysis

The ILM thickness for each of the specimens was measured and calculated as the mean from 20 randomly selected regions. The number of cell fragments adhering to the ILM, which was defined as the number of the cell fragments per unit area of ILM that was 100 μm^2 in size, was counted and computed in four areas of each of the specimens as described above. The total volume of cell fragments per unit area of ILM that was 100 μm^2 in size was also measured in four areas of each of the specimens. The mean cell fragment volume was calculated as the total volume of the cell fragments divided by the number of cell fragments in each of the specimens.

In both the ERM and the MH groups, patient age, ILM thickness, the number of cell fragments per unit area of the ILM, the total volume of cell fragments per unit area of ILM, and the mean cell fragment volume are presented as the mean ± standard deviation. The statistical significance of the differences was analyzed by means of a paired *t*-test between the pre- and postoperative visual acuity in both groups and the pre- and postoperative foveal thickness in the ERM group. An unpaired *t*-test was used to analyze the ILM thickness and the mean cell fragment volume between the two groups, whereas the Mann-Whitney *U* test was used to analyze the number of cell fragments per unit area of the ILM and the total volume of the cell fragments per unit area of the ILM between the two groups. All calculations were performed using Prism 7 for Mac OS X (version 7.0b; GraphPad Software, Inc., San Diego, CA), with *P* values less than 0.05 considered significant.

Results

All six of the MH group patients showed closure of the MH after the surgery, with the visual acuity improving significantly from a logMAR of 0.49 ± 0.19 to 0.12 ± 0.12 at 12 months after the surgery ($P = 0.004$, paired *t*-test; Table). The ILM obtained during surgery for MH showed homogenous dense reticular membranous tissue in the observed sections (Figs. 2A, 2B). At the vitreal side of the ILM, the surface was smooth, without any apparent cellular components. In contrast, on the retinal side, which was characterized by an undulated surface, small, round fragments of cells were seen in all specimens.

The three-dimensional view, which was created by segmentation of the ILM and the cell fragments, revealed the presence of a smooth surface on the vitreal side of the ILM (Fig. 2C). However, the numerous cell fragments varied from round to stellate in shape and were scattered on the retinal surface of the ILM (Fig. 2D). No specialized structure, such as neurotubules or neurofilaments, was detected inside the cell fragments. The mean ILM thickness was 2.69 ± 0.31 μm. The number of cell fragments per unit area of ILM was 5.07 ± 1.03/100 μm^2. The total volume of cell fragments per unit area of ILM was 3.54 ± 1.24 μm^3/100 μm^2. The mean volume of the cell fragment was 0.70 ± 0.20 μm^3.

All six of the ERM group patients exhibited a significant decrease in the macular thickness from 453.3 ± 41.6 to 338.3 ± 28.8 μm, and a significant improvement in the visual acuity from a logMAR of 0.27 ± 0.10 to 0.06 ± 0.06 at 12 months after the surgery ($P = 0.001$ and $P = 0.003$, respectively, paired *t*-test; Table). Similar to the ILM observed in the MH group, the ILM in the ERM group also presented with homogenous dense membranous tissue in the observed sections (Figs. 3A, 3B). Although fibrous and cellular components of ERM adhered at the vitreal side of the ILM, the smooth surface of the ILM distinguished it from the ERM (Fig. 3B). The retinal surface of the ILM exhibited numerous undulations of the ILM and the adherence of cell fragments (Figs. 3A, 3B). In the three-dimensional view, the vitreal surface of the ILM beneath the ERM exhibited a smooth surface (Fig. 3C). On the retinal surface of the ILM, there were numerous cell fragments present that varied in shape from round to stellate (Fig. 3D). Large cell bodies with sizes ranging from 4.6 to 6.2 μm in diameter were found in three out of the 24 observed areas in the six ERM group specimens (Fig. 4). Mean ILM thickness in the ERM group was 3.07 ± 0.21 μm, which was significantly thicker than that observed in the MH group ($P = 0.030$, unpaired *t*-test). The number of cell fragments per unit area of ILM was 12.85 ± 3.45/100 μm^2. The total volume of the cell fragments per unit area of ILM was 10.45 ± 2.77 μm^3/100 μm^2. Both of these values were significantly higher than those found in the MH group ($P = 0.0024$ and $P = 0.0022$, respectively, Mann-Whitney *U* test). The mean volume of the cell fragment was 0.822 ± 0.109 μm^3, which did not differ from that in the MH group ($P = 0.245$, unpaired *t*-test).

Discussion

Although previous TEM studies have demonstrated the appearance of cell fragments on the peeled

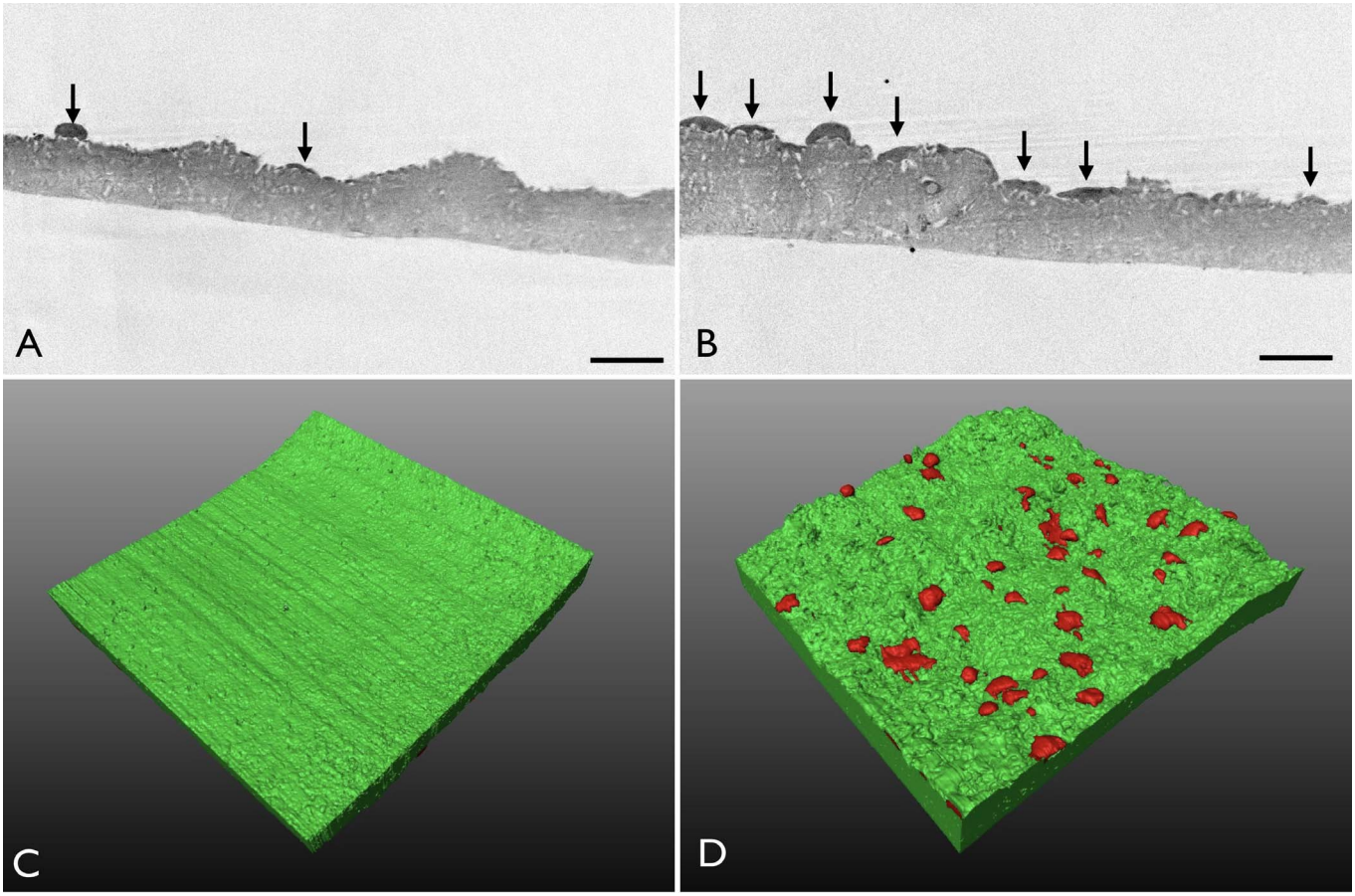

Figure 2. Serial sections and three-dimensional reconstruction of the ILM obtained during surgery for MH. (A, B) Serial sections of the ILM. Round cell fragments adhered to the ILM (*arrows*). *Scale bar*: 2 μm. (C) Three-dimensional view of the vitreal side of the ILM. Note the smooth surface. (D) Three-dimensional view of the retinal side of the ILM. Round cell fragments were observed. *Red*, cell fragments; *green*, ILM.

ILM, it has been difficult to interpret the entire shape of the cell fragments and quantitatively analyze them by sections.[16,17,28–33] Steel et al.[34] demonstrated quantifying the amount of the cell debris on the surface of the ILM by using the method of superimposing a grid of lines on the image. Our present study demonstrated that FIB/SEM was able to determine three-dimensional images of the ILM and the adhering cell fragments, thereby making it possible to perform a quantitative analysis.

For all of the specimens from the MH group in this study, the surface at the vitreal side of the ILM was smooth without any apparent cellular components. This was in contrast to the fibrous and cellular components of the ERM that adhered to the vitreal side of the ILM in the ERM group. Based on the OCT findings, we carefully selected the patients with MH, all of whom were stage 2 or 3 without apparent ERM. In fact, the brilliant blue G staining pattern observed during the surgery was uniform in all of the patients, which indicated that the vitreous had been completely removed by the artificial separation of the posterior vitreous during the vitrectomy.[34,35]

In contrast, all of the specimens from both the MH and ERM groups showed cell fragments on the retinal side of the ILM. Furthermore, our results also revealed that peeled ILM in the ERM group exhibited a greater number of cell fragments adhered to the ILM compared to that in the MH group. It is likely that the cell fragments on the ILM were undoubtedly caused by mechanical trauma. However, as hypothesized in a previous report, the observed difference between these two groups might be due to alterations of cell–cell or cell–substrate attachments or due to changes of the retinal surface structure from a smooth surface to a folded surface in ERM.[33] In fact, the thicker ILM observed in the ERM group might be

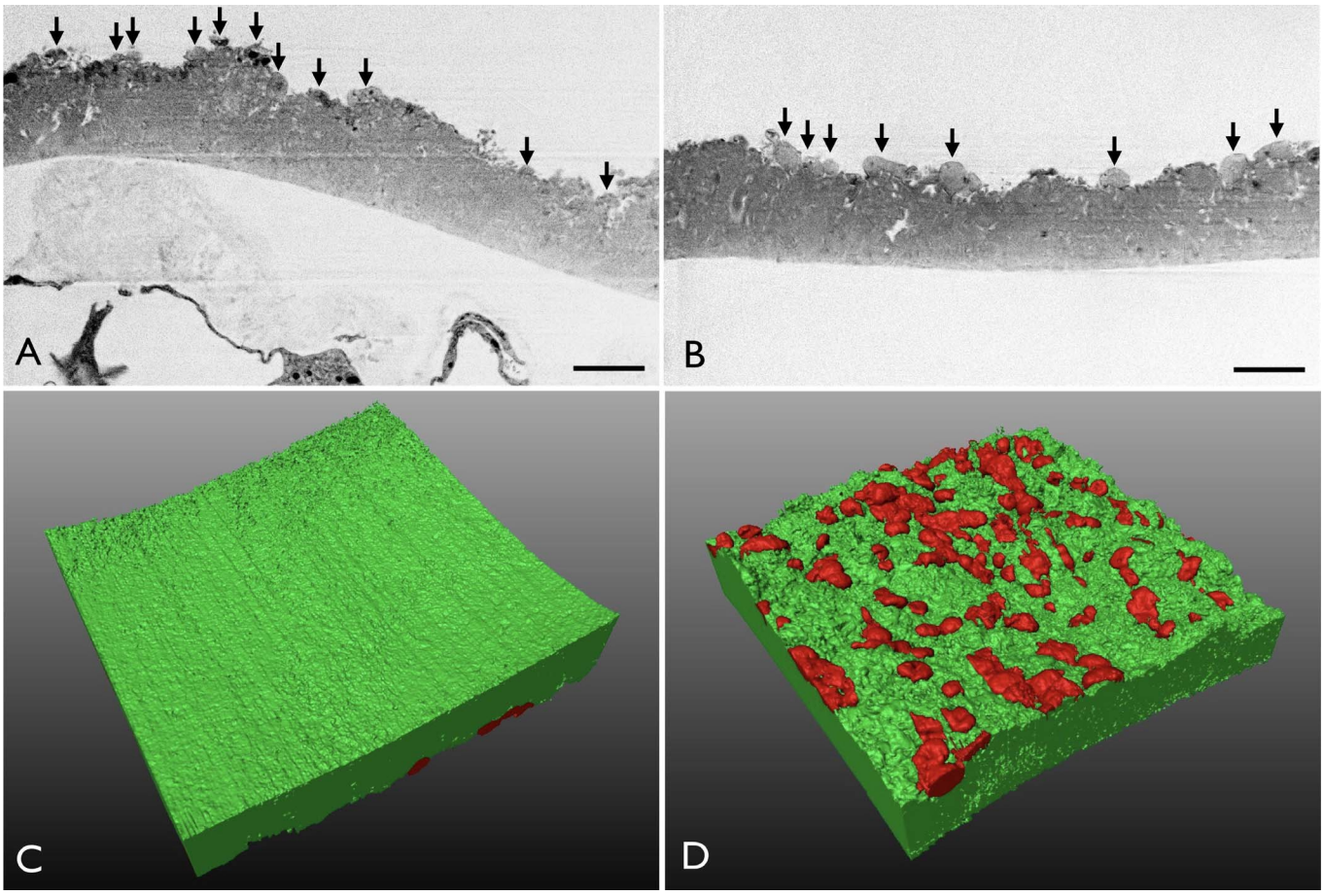

Figure 3. Serial sections and three-dimensional reconstruction of the ILM obtained during surgery for ERM. (A, B) Serial sections of the ILM. Numerous cell fragments adhered to the ILM (*arrows*). *Scale bar*: 2 μm. (C) Three-dimensional view of the vitreal side of the ILM. Note the smooth surface. ERM is omitted in the three-dimensional view. (D) Three-dimensional view of the retinal side of the ILM. Variously shaped cell fragments were observed. *Red*, cell fragments; *green*, ILM.

indicative of an increased content of extracellular matrices, as has been described in ERM or diabetic maculopathy.[31,35] It was not possible to detect the specific extracellular matrices, such as elastin fibers, in the specimens in this study.

Chen et al.[13] reported that while inner nuclear layer microcysts were frequently induced shortly after surgery in ERM patients, which included both ERM and ILM peeling, this retinal change was rarely observed in the MH patients after surgery. Thus, these authors hypothesized that the inner nuclear layer microcysts may result from impaired Müller cell functioning or cell degeneration in the inner nuclear layer secondary to the mechanical stretching of the retina by the more severe, acute form of ERM and the surgery itself. Our present study demonstrated that ILM peeling in the ERM patients resulted in more severe inner retinal damage. Therefore, both the indication for and the technique of the ILM peeling in the ERM patients should be carefully considered prior to performing the procedure.

One possible strategy for reducing the mechanical retinal trauma associated with the ILM peeling might be to use a pharmacologic agent that causes loosening of the ILM and the underlying cells. In fact, an ultrastructural study of ILM peeling following an injection of the recombinant truncated form of the human serine protease plasmin, ocriplasmin, has revealed that there was no retinal cell debris or cell fragments on the retinal side of the ILM.[32] In contrast, Steel et al.[36] reported that the ILM removed during vitrectomy after ocriplasmin treatment did not show any changes compared with that found for the untreated control. They speculated that it is possible that even if disrupted by ocriplasmin, the adhesion molecules could have reformed by the time of the actual vitrectomy surgery.

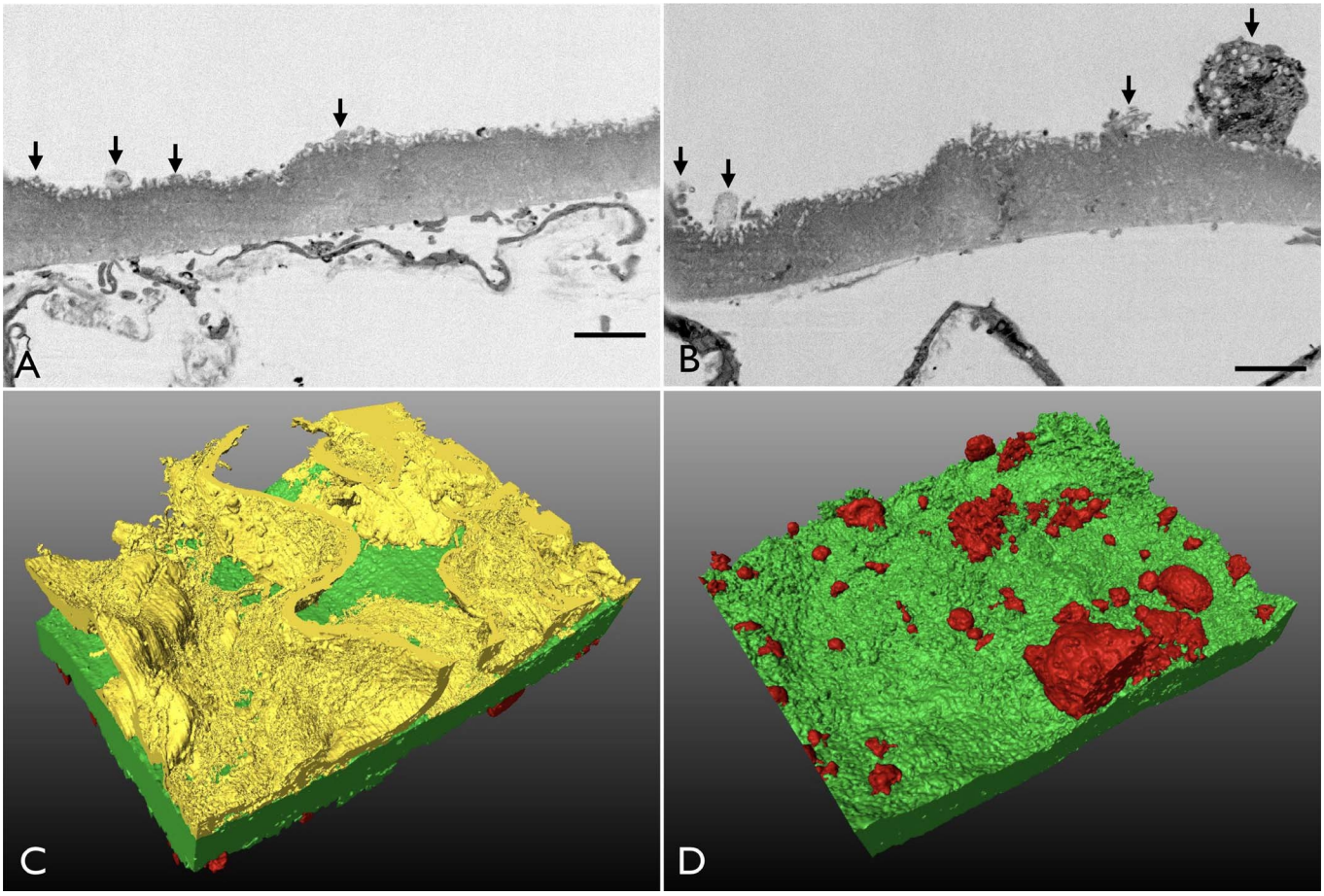

Figure 4. Another example of the serial sections and three-dimensional reconstruction of the ILM for ERM. (A, B) Serial sections of the ILM. Numerous cell fragments adhered to the ILM (*arrows*). *Scale bar*: 2 μm. (C) Three-dimensional view of the vitreal side of the ERM and ILM. Note the ERM attached to the ILM. (D) Three-dimensional view of the retinal side of the ILM. Various cell fragment shapes were observed. Note the cell body on the ILM. *Red*, cell fragments; *green*, ILM; *yellow*, ERM.

Another feasible strategy for reducing the retinal trauma by ILM peeling is through the use of ILM abrasion with a diamond-dusted membrane scraper. This technique avoids the complete removal of the retinal ILM basement membrane and subjacent tissues. Results for this procedure appear to provide MH closure rates similar to those found for traditional ILM peeling.[35,37]

There were several limitations for our current study. First, even though there was a statistical difference between the MH and ERM groups, only a small number of specimens were investigated in our study. Second, it was not possible to definitively determine the origin of the cell fragments that were adhering to the ILM. This was especially the case for the difference in the cell type between the groups. Although most of the cell fragments indicate Müller cell origin, the presence of other glial or neural cells could not be ruled out, even though we could not detect any obvious structure of neurotubules or neurofilaments that indicated the nerve fiber layer.

Further investigations will need to be undertaken in order to clarify the effects of the ILM peeling on other macular diseases, such as macular edema, macular retinoschisis, or macular pucker. In addition, the procedural differences in the ILM peeling during surgery, such as the peeling speed or the type of dye used, will also need to be investigated.

In conclusion, the present results that showed that all of the ILM obtained during surgery exhibited cell fragments may indicate that ILM peeling led to retinal damage during the surgery. The actual degree of the damage could differ and be dependent on the underlying macular diseases. Compared to MH, ILM peeling for ERM might be associated with a higher risk of retinal damage.

Acknowledgments

This work was supported by JSPS KAKENHI Grant JP15K10886 and JP16H06280.

Disclosure: **A. Hirata**, None; **K. Murata**, None; **K. Hayashi**, None; **K. Nakamura**, None

References

1. Brooks HL Jr. Macular hole surgery with and without internal limiting membrane peeling. *Ophthalmology*. 2000;107:1939–1948.
2. Park DW, Lee JH, Min WK. The use of internal limiting membrane maculorrhexis in treatment of idiopathic macular holes. *Korean J Ophthalmol*. 1998;12:92–97.
3. Haritoglou C, Gandorfer A, Gass CA, Schaumberger M, Ulbig MW, Kampik A. The effect of indocyanine-green on functional outcome of macular pucker surgery. *Am J Ophthalmol*. 2003;135:328–337.
4. Li K, Wong D, Hiscott P, Stanga P, Groenewald C, McGalliard J. Trypan blue staining of internal limiting membrane and epiretinal membrane during vitrectomy: visual results and histopathological findings. *Br J Ophthalmol*. 2003;87:216–219.
5. Gandorfer A, Messmer EM, Ulbig MW, Kampik A. Indocyanine green selectively stains the internal limiting membrane. *Am J Ophthalmol*. 2001;131:387–388.
6. Avci R, Kaderli B, Avci B, et al. Pars plana vitrectomy and removal of the internal limiting membrane in the treatment of chronic macular oedema. *Graefes Arch Clin Exp Ophthalmol*. 2004; 242:845–852.
7. Ikuno Y, Sayanagi K, Ohji M, et al. Vitrectomy and internal limiting membrane peeling for myopic foveoschisis. *Am J Ophthalmol*. 2004; 137:719–724.
8. Mester V, Kuhn F. Internal limiting membrane removal in the management of full-thickness macular holes. *Am J Ophthalmol*. 2000;129:769–777.
9. Schechet SA, DeVience E, Thompson JT. The effect of internal limiting membrane peeling on idiopathic epiretinal membrane surgery, with a review of the literature. *Retina*. 2017;37:873–880.
10. Dehghan MH, Salehipour M, Naghib J, Babaeian M, Karimi S, Yaseri M. Pars plana vitrectomy with internal limiting membrane peeling for refractory diffuse diabetic macular edema. *J Ophthalmic Vis Res*. 2010;5:162–167.
11. Mitamura Y, Ohtsuka K. Relationship of dissociated optic nerve fiber layer appearance to internal limiting membrane peeling. *Ophthalmology*. 2005;112:1766–1770.
12. Sabry D, El-Kannishy A, Kamel R, Abou Samra W. Correlation between en face optical coherence tomography defects of the inner retinal layers and ganglion cell inner plexiform layer analysis after internal limiting membrane peeling for idiopathic full-thickness macular hole. *Invest Ophthalmol Vis Sci*. 2016;57:OCT444–450.
13. Chen SJ, Tsai FY, Liu HC, Chung YC, Lin TC. Postoperative inner nuclear layer microcysts affecting long-term visual outcomes after epiretinal membrane surgery. *Retina*. 2016;36:2377–2383.
14. Terasaki H, Miyake Y, Nomura R, et al. Focal macular ERGs in eyes after removal of macular ILM during macular hole surgery. *Invest Ophthalmol Vis Sci*. 2001;42:229–234.
15. Lim JW, Cho JH, Kim HK. Assessment of macular function by multifocal electroretinography following epiretinal membrane surgery with internal limiting membrane peeling. *Clin Ophthalmol*. 2010;4:689–694.
16. Konstantinidis L, Uffer S, Bovey EH. Ultrastructural changes of the internal limiting membrane removed during indocyanine green assisted peeling versus conventional surgery for idiopathic macular epiretinal membrane. *Retina*. 2009;29: 380–386.
17. Schumann RG, Remy M, Grueterich M, Gandorfer A, Haritoglou C. How it appears: electron microscopic evaluation of internal limiting membrane specimens obtained during brilliant blue G assisted macular hole surgery. *Br J Ophthalmol*. 2008;92:330–331.
18. Nakamura T, Murata T, Hisatomi T, et al. Ultrastructure of the vitreoretinal interface following the removal of the internal limiting membrane using indocyanine green. *Curr Eye Res*. 2003;27:395–399.
19. Knott G, Marchman H, Wall D, Lich B. Serial section scanning electron microscopy of adult brain tissue using focused ion beam milling. *J Neurosci*. 2008;28:2959–2964.
20. Bushby AJ, P'Ng KM, Young RD, Pinali C, Knupp C, Quantock AJ. Imaging three-dimensional tissue architectures by focused ion beam scanning electron microscopy. *Nat Protoc*. 2011; 6:845–858.

21. Knott G, Rosset S, Cantoni M. Focussed ion beam milling and scanning electron microscopy of brain tissue. *J Vis Exp*. 2011;e2588.
22. Schmidt F, Kuhbacher M, Gross U, Kyriakopoulos A, Schubert H, Zehbe R. From 2D slices to 3D volumes: image based reconstruction and morphological characterization of hippocampal cells on charged and uncharged surfaces using FIB/SEM serial sectioning. *Ultramicroscopy*. 2011;111:259–266.
23. Enaida H, Ishibashi T. Brilliant blue in vitreoretinal surgery. *Dev Ophthalmol*. 2008;42:115–125.
24. Hirashima S, Ohta K, Kanazawa T, et al. Three-dimensional ultrastructural analysis of cells in the periodontal ligament using focused ion beam/scanning electron microscope tomography. *Sci Rep*. 2016;6:39435.
25. Ohta K, Sadayama S, Togo A, Higashi R, Tanoue R, Nakamura K. Beam deceleration for block-face scanning electron microscopy of embedded biological tissue. *Micron*. 2012;43:612–620.
26. Yoshitomi M, Ohta K, Kanazawa T, et al. Three-dimensional ultrastructural analyses of anterior pituitary gland expose spatial relationships between endocrine cell secretory granule localization and capillary distribution. *Sci Rep*. 2016;6:36019.
27. Walton J. Lead aspartate, an en bloc contrast stain particularly useful for ultrastructural enzymology. *J Histochem Cytochem*. 1979;27:1337–1342.
28. Beyazyildiz O, Tirhis MH, Hekimoglu ER, et al. Histopathological analysis of internal limiting membrane surgically peeled from eyes with epiretinal membrane. *Curr Eye Res*. 2016;41:258–265.
29. Haritoglou C, Gandorfer A, Gass CA, Kampik A. Histology of the vitreoretinal interface after staining of the internal limiting membrane using glucose 5% diluted indocyanine and infracyanine green. *Am J Ophthalmol*. 2004;137:345–348.
30. Kwok AK, Lai TY, Yew DT, Li WW. Internal limiting membrane staining with various concentrations of indocyanine green dye under air in macular surgeries. *Am J Ophthalmol*. 2003;136:223–230.
31. Matsunaga N, Ozeki H, Hirabayashi Y, Shimada S, Ogura Y. Histopathologic evaluation of the internal limiting membrane surgically excised from eyes with diabetic maculopathy. *Retina*. 2005;25:311–316.
32. Schumann RG, Wolf A, Mayer WJ, et al. Pathology of internal limiting membrane specimens following intravitreal injection of ocriplasmin. *Am J Ophthalmol*. 2015;160:767–778.
33. Schumann RG, Yang Y, Haritoglou C, et al. Histopathology of internal limiting membrane peeling in traction induced maculopathies. *J Clin Exp Ophthalmol*. 2015;3:e1–6.
34. Steel DH, Dinah C, Madi HA, White K, Rees J. The staining pattern of brilliant blue G during macular hole surgery: a clinicopathologic study. *Invest Ophthalmol Vis Sci*. 2014;55:5924–5931.
35. Almeida DR, Chin EK, Tarantola RM, et al. Effect of internal limiting membrane abrasion on retinal tissues in macular holes. *Invest Ophthalmol Vis Sci*. 2015;56:2783–2789.
36. Steel DH, Sandinha MT, White K. The plane of vitreoretinal separation and results of vitrectomy surgery in patients given ocriplasmin for idiopathic macular hole. *Invest Ophthalmol Vis Sci*. 2015;56:4038–4044.
37. Mahajan VB, Chin EK, Tarantola RM, et al. Macular hole closure with internal limiting membrane abrasion technique. *JAMA Ophthalmol*. 2015;133:635–641.